Journal of The Electrochemical Society, **149** (6) A765-A772 (2002)
0013-4651/2002/149(6)/A765/8/$7.00 © The Electrochemical Society, Inc.

Influence of Anode Flow Rate and Cathode Oxygen Pressure on CO Poisoning of Proton Exchange Membrane Fuel Cells

Jingxin Zhang,* Tony Thampan, and Ravindra Datta,z**

Fuel Cell Center, Department of Chemical Engineering, Worcester Polytechnic Institute, Worcester, Massachusetts 01609, USA

The anode flow rate of a proton exchange membrane (PEM) fuel cell involving Pt anode electrocatalyst is found to strongly influence the single cell performance when H_2 containing trace amounts of CO is used as the feed. The performance drops dramatically due to CO poisoning as the anode flow rate increases until a large overpotential is reached when it levels off. This effect of the flow rate on the extent of poisoning is found to be reversible and is explained as depending on the actual concentration of CO in the anode chamber which in turn depends on the feed content, the flow rate, and CO oxidation kinetics on Pt. Further, it is found that oxygen permeating across the PEM from the cathode side also appreciably affects the anode overpotential by providing another route for CO oxidation. A CO inventory model is provided that explains the observed phenomena in a PEM fuel cell operating with H_2/CO as anode feed and a cathode feed with different oxygen pressures.
 [DOI: 10.1149/1.1475686]

Manuscript submitted June 20, 2001; revised manuscript received January 2, 2002. Available electronically April 25, 2002.

Proton exchange membrane (PEM) fuel cells power plants for stationary and mobile applications are planned to be operated on reformate gas feed that would inevitably contain trace amounts of CO.[1,2] Extensive investigations have been performed to evaluate the CO tolerance of the PEM fuel cells with different electrocatalysts and under different conditions. It has been reported that the fuel cell temperature and CO content of the gas mixture are the key parameters that determine the performance of a given catalyst.[3-8] The poisoning effect of CO has also been investigated in electrochemical cells incorporating liquid electrolytes such as H_3PO_4 or H_2SO_4.[9-12] These investigations provide much insight into the effect of CO poisoning on the performance of PEM fuel cells. The present work is motivated by our desire to systematically study the mechanisms and kinetics of standard fuel cell catalyst, such as Pt and PtRu, at real PEM fuel cell conditions. During the study of CO poisoning on PEM fuel cell performance with Pt anode catalyst, we found the strong influence of certain operating parameters, namely the anode flow rate and cathode oxygen partial pressure, which have not so far been documented.

The performance of a single fuel cell is normally studied in the laboratory under a constant flow rate or stoichiometry. Though PEM fuel cell anodes fed with pure H_2 are often operated near a stoichiometry of one, reformate gas mixtures from catalytic reformers require higher flow rates, because considerable amounts of CO_2 and N_2 are also present in the gas mixtures, with H_2 concentrations ranging from 40 to 75% depending upon the reforming system and specific process.[13] It is shown in this work that the anode flow rate and cathode oxygen partial pressure are very important operating parameters influencing the extent of CO poisoning when operating with a feed containing essentially pure H_2 along with trace amounts of CO. We report here for the first time, experimental results on the effect of anode flow rate and cathode oxygen partial pressure on the performance of a single PEM fuel cell with Pt anode catalyst at different temperatures. These results are of significance both practically and fundamentally for a single cell as well as for stacks.

In modeling and experimental studies of H_2/CO oxidation on Pt anode in PEM fuel cells, it is often tacitly assumed that the CO concentration in the anode chamber is identical to that in the inlet feed. This, of course, is not true due to CO oxidation on Pt, especially when the anode inlet flow rate is small (low stoichiometry). Under these conditions, it is necessary to write an overall CO mass balance including terms for the rate of CO oxidation in addition to those for flow in and out so that the performance of the Pt catalyst toward CO oxidation can be objectively evaluated. A preliminary CO_x inventory model has been put forth by Bellows *et al.*,[7] where the change of surface coverage of CO was attributed to CO adsorption, CO electro-oxidation, and CO_2 reduction (in a simulated reformate gas). They assumed CO adsorption onto Pt to be kinetically very rapid and approaching a complete monolayer coverage for concentrations as low as 1 ppm.[7]

In the work reported here, the anode inlet flow rate and cathode oxygen partial pressure are found to dramatically influence the anode overpotential, and consequently the overall fuel cell performance. A more complete and quantitative inventory of CO in the anode side is, therefore, necessary, which is provided here to account for the effect of anode flow rate as well as cathode oxygen partial pressure on the PEM fuel cell performance.

Experimental

The 20 wt % Pt/C catalyst powder used to prepare the anode was purchased from E-TEK Inc. (Natick, MA). Gas diffusion electrodes already loaded with 20 wt % Pt/C at a metal loading of 0.4 mg/cm^2, were also purchased from E-TEK. Nafion® 115 and 117 proton-exchange membranes (DuPont, Fayetteville, PA) were used after sequential treatment with 2% H_2O_2, deionized water, 0.5 M H_2SO_4, and again with deionized water in order to remove any inorganic and organic impurities. The membrane electrode assembly (MEA) was prepared by hot-pressing in a model C Carver hot press at 130°C and under a pressure of 4000 lb for about 2 min. The MEA was then incorporated in a 5 cm^2 single cell from ElectroChem, Inc. (Woburn, MA), and tested in a test station with temperature, pressure, humidity, and flow rate control. The current-voltage characteristics were recorded using a HP 6060B DC electronic load, interfaced with a PC using LabView software (National Instruments, Austin, TX).

The single fuel cell was tested at different temperatures, different anode flow rates, and different cathode oxygen pressures. Anode and cathode gases were first humidified through a stainless steel bottle containing water at a desired temperature before being fed into the fuel cell. The temperatures of the humidification bottles were set at 15 and 10°C higher than that of the fuel cell for the anode and cathode side, respectively. The total pressure of both anode and cathode side was maintained at 30 psig unless otherwise noted. The experiment was conducted continuously, with some data being collected for as long as 20 h to insure a steady-state value. The flow rates reported in this study are all at the standard state (1 atm and 25°C) and in units of standard cubic centimeter per minute (sccm). Premixed H_2/108 ppm CO was purchased from MG Industries (Morrisville, PA). The CO concentration was certified by the supplier and was not independently confirmed. The fuel cell performance results reported here are all with H_2/108 ppm CO; Pt loading,

* Electrochemical Society Student Member.
** Electrochemical Society Active Member.
z E-mail: rdatta@wpi.edu

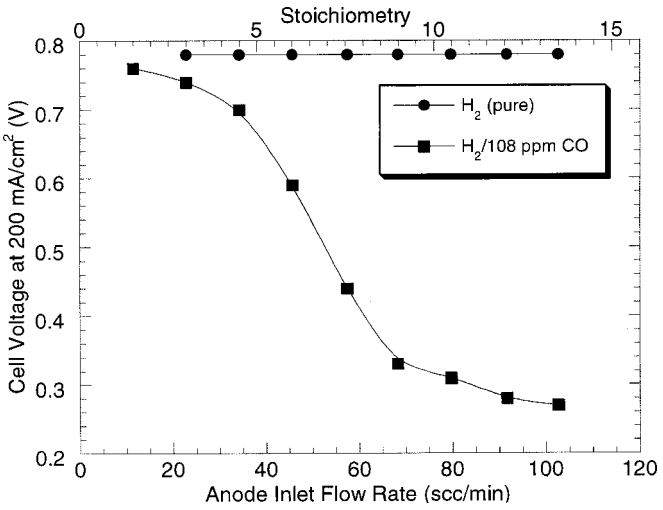

Figure 1. Effect of anode flow rate on cell voltage at constant current density for H_2 and H_2/108 ppm CO for 5 cm^2 PEM fuel cell at 80°C; Nafion 115 membrane. Current density, 200 mA/cm^2.

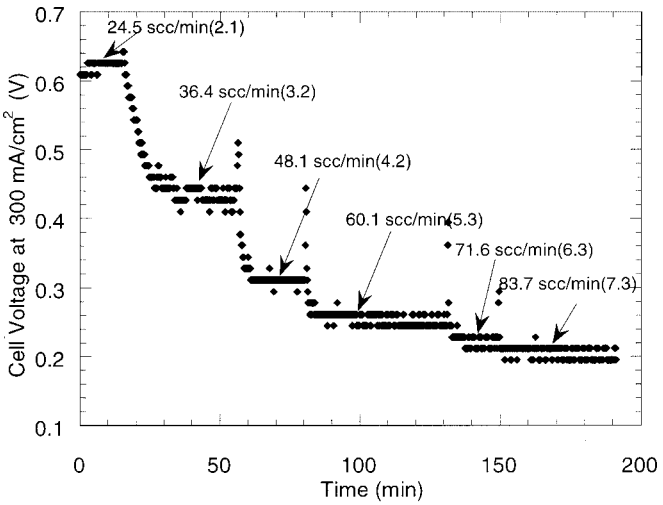

Figure 2. Cell voltage profile at different anode inlet flow rates at 300 mA/cm^2 at 80°C; Nafion 115 membrane. Numbers in parentheses are the corresponding stoichiometry.

0.4 mg/cm^2 (20% Pt/C); 80°C; and Nafion 115 membrane, unless otherwise noted.

Results

Effect of anode flow rate.—Figure 1 shows the steady-state results of the change of cell voltage with anode flow rate at 80°C and a constant current density of 200 mA/cm^2. The data for pure H_2 (without any CO) under identical conditions are also plotted for comparison. The upper abscissa in Fig. 1 shows the corresponding stoichiometry for the current density of 200 mA/cm^2. As expected, the cell voltage is not influenced by the flow rate for the case of pure H_2. However, it is dramatically influenced by the anode flow rate when operating with H_2/CO (108 ppm) mixture. At relatively small flow rates, the cell voltage deviation from that of pure H_2 is rather small. Thereafter, there is a region where the cell voltage drops precipitously with an increase of the anode flow rate. However, at relatively large flow rates, a plateau of the cell voltage is reached, and a further increase of the anode flow rate does not significantly affect the cell voltage. These observations are explained below on the basis of the increasing CO content in the anode chamber to which the MEA is exposed with the flow rate, eventually approaching feed concentration at high flow rates. This is due to the mass balance accounting for CO entering and exiting the anode chamber via flow as well as that consumed via oxidation on Pt by water and oxygen diffusing through the PEM from the cathode.

In a study of transient CO poisoning by Bauman *et al.*,[14] the time it took to attain steady-state current when switched from one CO content feed to another was found to be influenced by the anode flow rate. The higher the flow rate, the shorter the time it took for the cell to reach steady state. However, little difference was found in the steady-state current for the flow rate of 1.5 stoichiometry *vs.* 3.0 stoichiometry (Fig. 4, Ref. 14). Actually, this stoichiometry corresponds to the current before CO poisoning. Since after the introduction of CO, the cell current density drops from 960 mA/cm^2 to about 120-140 mA/cm^2, the experimental stoichiometry for the current is nearly 10 rather than 1.5 which corresponds to the higher flow rate region of Fig. 1, where the cell performance has low sensitivity to the change in anode flow rate.

Cell voltage *vs.* time data are shown in Fig. 2 over a period of more than 3 h with the fuel cell operating at 80°C and a current density of 300 mA/cm^2 when several equal step changes were introduced in the flow rate. The cell voltage data were continuously collected for these step changes. After each adjustment, it is seen in Fig. 2 that within a few minutes the fuel cell attains a steady-state cell voltage corresponding to the new anode flow rate. The cell voltage remains fairly stable at various flow rates (±20 mV). This figure also shows the dramatic cell voltage change in the initial step increase of the anode inlet flow rate, with increasingly smaller changes for subsequent step changes of equivalent size. The scattered points between the different step changes are due to the rapid voltage recovery during the brief period of resetting of the anode flow rate from one value to another.

In order to further investigate the transient recovery behavior, the anode inlet feed valve was shut off after the cell reached a steady state corresponding to the given anode flow rate. The ensuing cell voltage recovery *vs.* time is shown in Fig. 3, followed by the cell repoisoning and voltage decline when the H_2/CO feed is reintroduced at the original flow rate. It should be pointed out that in this transient experiment, when the H_2/CO feed was stopped, the total pressure of the anode chamber would drop gradually below 30 psig due to the consumption of H_2 to sustain a certain current density. It

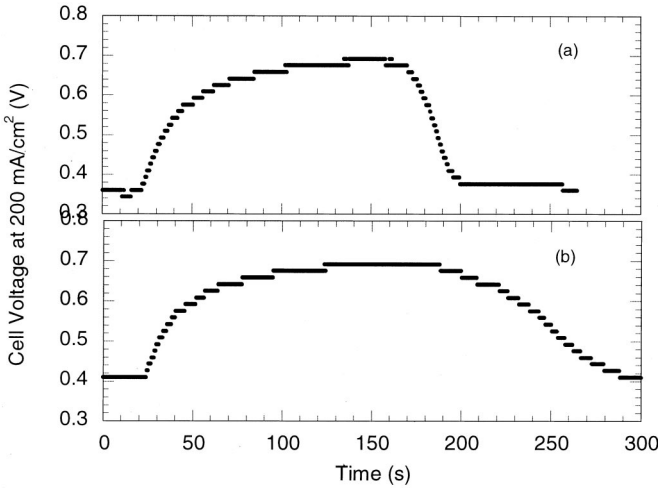

Figure 3. Recovery and poisoning transient for the cell operated at 200 mA/cm^2 at 80°C for different anode inlet flow rates. (a) 80 and (b) 57.5 sccm. Nafion 115 membrane.

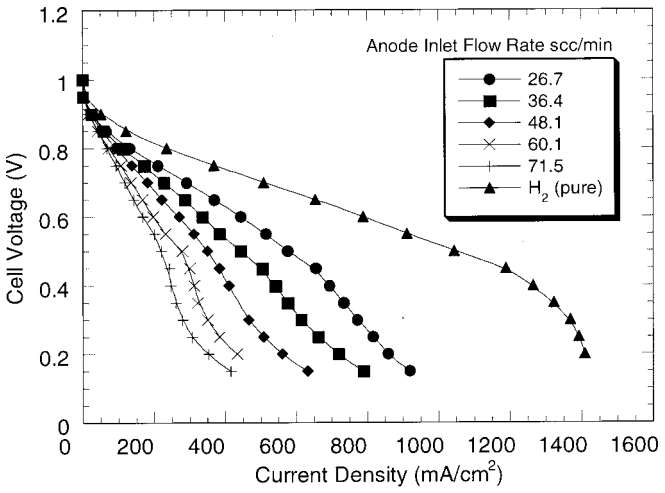

Figure 4. PEM fuel cell performance at different anode flow rates at 80°C; Nafion 115 membrane.

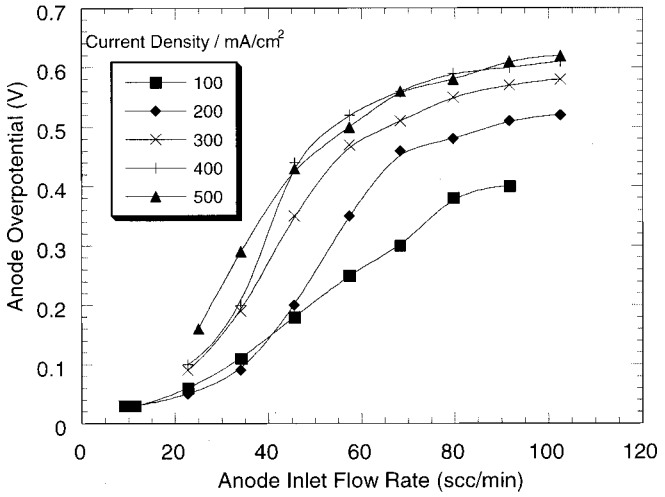

Figure 5. Anode overpotential *vs.* flow rate at different current density at 80°C; Nafion 115 membrane.

is seen from Fig. 3 that the cell voltage recovers fully within a minute or two upon valve closure. After the anode gas is reintroduced, the cell voltage decreases rapidly to the value prior to valve closure. These results indicate that CO poisoning is highly reversible and rapid. It is also noteworthy that the time of poisoning to a steady-state voltage after the introducing of H_2/CO is dependent on the anode inlet flow rate. The higher the inlet flow rate, the shorter the transient time to reach the steady-state voltage. In Fig. 3, the transient time decreased from about 110 s to about 50 s when the inlet flow rate was increased from 57.5 sccm (Fig. 3b) to 80 sccm (Fig. 3a). These results are in agreement with those of Bauman *et al.*,[14] who observed a transient period of less than 300 s. These periods are also of the order of the time constant for the anode chamber, the mass transfer and kinetics of the CO adsorption on Pt in PEM fuel cell anode being much more rapid. This aspect is further discussed below.

More detailed current-voltage characteristics for the PEM fuel cell at 80°C are shown in Fig. 4. The performance curve for pure H_2 is also plotted for comparison. We use the same protocol to get the performance curve for H_2/CO as we did with pure H_2. Namely, when the anode flow rate is set at a given value, the current is monitored at a cell voltage of 0.4 V until the current is stable. Then the current is measured for different cell voltages. At each cell voltage, the current is recorded in about 1 min after the voltage settings. The curves shown in Fig. 4 were obtained at different anode flow rates and clearly demonstrate the remarkable effect of flow rate on the cell performance. Interestingly, the current-voltage curves exhibit trends that are qualitatively similar to those with H_2/CO gas mixtures of different CO content.[3,4] At low current densities, the difference between the cell voltage at different flow rates at a given current density is small. With an increase in current density, the deviation becomes increasingly large. Furthermore, it may be noticed that there are three regions with different slopes in the current-voltage curves. The slope at low current densities is smaller than that at relatively higher current densities. But below about 0.2 V for the high current density region, the slope of curves at different flow rates becomes smaller again. The similarity between the effect of flow rate for a given CO content and that of a CO content at a constant flow rate is not coincidental, as explained later. The CO content to which the MEA is exposed is, in fact, dependent upon the flow rate.

We further note that the performance reported here at low flow rates is better than that reported in the literature for similar CO contents.[3,4,8] Typically, the flow rates in these studies are larger and correspond to the large stoichoimetry flow rate region of this study. The performance reported in the literature is in good agreement with our data for the higher flow rates.[6,8] Unfortunately, the flow rate values are often not reported in the literature.

Anode overpotential.—Overall fuel cell voltage is given by the following expression[15]

$$V = V_0 - \eta_A + \eta_C - i\left(\frac{L}{\sigma}\right) - i(R_I) \qquad [1]$$

where V_0 is the open-circuit potential, i is the current density, η_A and η_C are the anode and cathode overpotentials, respectively, L and σ are the thickness and conductivity of the proton-exchange membrane, respectively, while R_I is any interfacial resistance. Thus, at constant current density, the difference in the polarization of the anode between the cases of the presence ($\eta_{H_2/CO}$) and the absence of CO (η_{H_2}) in the anode feed can be obtained by making measurements of the cell voltage under otherwise identical experimental conditions except for the anode feed gas composition

$$\eta_{H_2/CO} - \eta_{H_2} = V_{H_2} - V_{H_2/CO} \qquad [2]$$

where V_{H_2} and $V_{H_2/CO}$ are the cell voltages with H_2 and H_2/CO, respectively. Further, since the overpotential for pure H_2 is small,[6,15] it may be neglected without substantial error. Thus, the anode overpotential in the presence of CO is assumed to be simply the cell voltage difference between the two cases, *i.e.*

$$\eta_{H_2/CO} \approx V_{H_2} - V_{H_2/CO} \qquad [3]$$

Figure 5 shows the thus calculated anode overpotential *vs.* flow rate at 80°C at different but constant values of current density. It is noteworthy that there are three relatively distinct regions in the anode overpotential curve. Below about 25 sccm, the anode overpotential rises slowly with the flow rate. In this range, only small current densities can be sustained. Above about 70 sccm, the anode overpotential also increases only gradually with the anode flow rate for all current densities. In the intermediate region between these values, the anode overpotential increases dramatically with flow rate. In this region at a given flow rate, the lower the current density, the smaller is the anode overpotential.

The change of anode overpotential with anode inlet flow rate at three different temperatures is compared in Fig. 6. It is clear that with the increase of the cell temperature, the maximum overpotential at relatively large flow rates decreases from about 0.7 V at 55°C to about 0.5 V at 80°C. Further, the transition of the anode overpo-

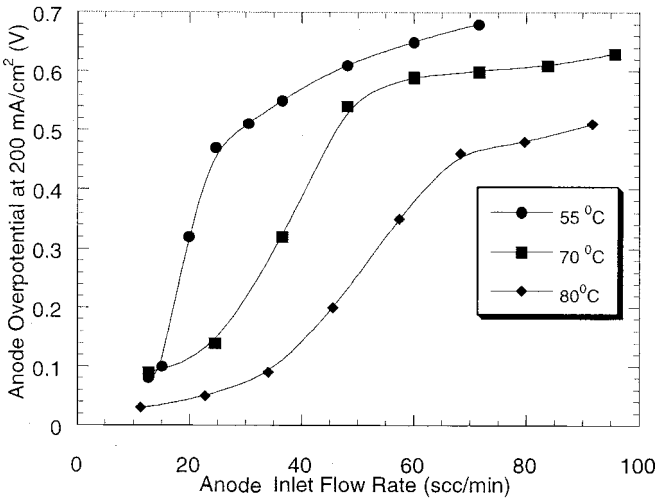

Figure 6. Anode overpotential *vs.* flow rate at 200 mA/cm^2 at different temperatures; Nafion 115 membrane.

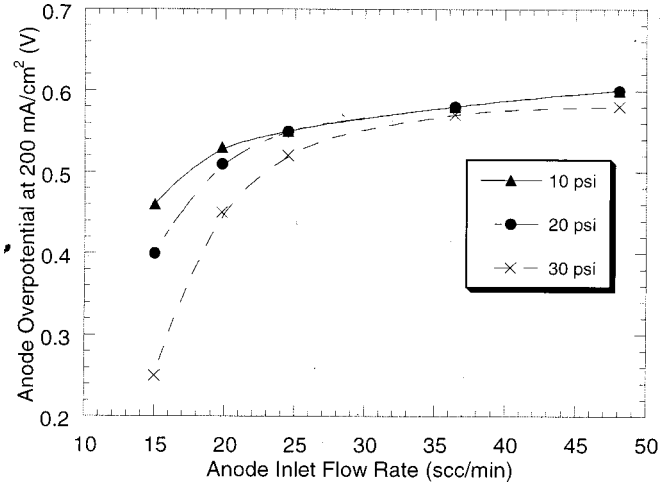

Figure 8. Anode overpotential *vs.* flow rate at 200 mA/cm^2 at different cathode O_2 pressures; 80°C; Nafion 117 membrane.

tential from a low value to a high value (the intermediate range) takes place at lower flow rates as temperature decreases. For example, threshold values of roughly 40 sccm at 80°C, 25 sccm at 70°C, and 15 sccm at 55°C are observed at 200 mA/cm^2.

Effect of oxygen pressure.—Experiments were also conducted under different cathode pressures using pure oxygen feed. The anode overpotential as a function of anode flow rate is thus plotted in Fig. 7 for three different cathode oxygen pressures. It is clear that the anode overpotential is substantially influenced by O_2 pressure, and it decreases as the cathode O_2 pressure increases. It should be pointed out that the cathode overpotential η_C is, of course, also a function of O_2 pressure.[15] In calculating anode overpotential, thus, the cell voltages V_{H_2} and $V_{H_2/CO}$ were both measured at the same O_2 pressures and subtracted according to Eq. 3.

It can be inferred from the above results that there must be some oxygen diffusing through the Nafion membrane to the anode side and contributing to the CO oxidation in addition to that by water. In order to further confirm this, Nafion 117 membrane was used in place of Nafion 115. Further, air was used in the cathode instead of pure O_2, with all the other components of the MEA and the operating conditions remained unchanged. The results are shown in Fig. 8 and 9, respectively. As apparent in Fig. 8, the cathode pressure for the case of the thicker Nafion 117 membrane is less influential as compared with the case of Nafion 115 membrane, with O_2 pressure affecting the overpotential mainly in the low flow rate region. When the anode overpotential is over 0.5 V, there is not any significant difference in the overpotential *vs.* flow rate at different O_2 pressures. When air is used in the cathode feed, the overpotential *vs.* the flow rate curve is virtually independent of the cathode pressure (Fig. 9). Further, the overpotential change with anode flow rate is over a narrower range as compared with the case of pure O_2, with the overpotential being high throughout, ranging from 0.5 to 0.6 V for all flow rates. Thus, when air is used, only a small amount of oxygen permeates and the electro-oxidation of CO via water is likely the dominant cleaning mechanism.

From these observations, it is virtually certain that any O_2 that permeates from cathode to anode plays an important role in the oxidative removal of CO and hence the observed anode flow rate effect. However, it is also apparent that O_2 is not the only agent of this CO removal. It is, thus, likely that the diffusing O_2 contributes to CO oxidation at lower anode overpotentials while water contributes to its electro-oxidation at higher anode overpotentials. For practical applications involving use of air at low pressures, the role of O_2 is less significant.

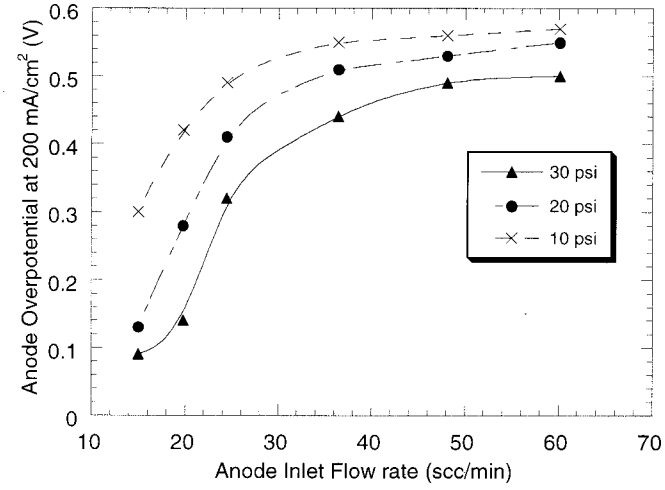

Figure 7. Anode overpotential *vs.* flow rate at 200 mA/cm^2 at different cathode O_2 pressures; 80°C; Nafion 115 membrane.

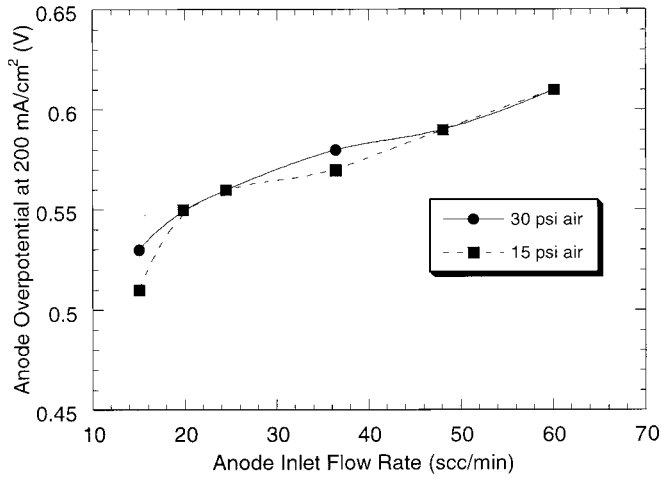

Figure 9. Anode overpotential *vs.* flow rate at 200 mA/cm^2 at different cathode air pressures; 80°C; Nafion 115 membrane.

Modeling

Mass balance.—The unsteady state material balance for species i in the anode chamber maybe written as[15]

$$V\frac{dc_i}{dt} = v_0 c_{i,0} - v c_i - N_i A \qquad [4]$$

where V is the volume of the electrode chamber, assumed here to be well-mixed, which is not an unreasonable assumption for a small ($5\ cm^2$) single cell. v_0 and v are the volumetric inlet and outlet anode flow rates, respectively. $c_{i,0}$ and c_i are the concentrations of species i in the inlet and outlet streams, respectively, N_i is the flux of species i into the MEA, and A is the geometric area of the MEA in the fuel cell. The flux N_i of H_2, CO, or any other species is, in principle, affected by mass-transfer limitations through the gas diffusion backing layer and catalyst layer as well as by the kinetics of the electrode reactions.[15] Bauman *et al.*[14] found that mass-transport barriers for CO are negligible. Our transient CO poisoning results further support this observation. Thus, mass transport limitations for CO are precluded as are those for H_2. In other words, the fluxes of CO as well as H_2 are assumed to be determined solely by the anode kinetics on Pt. Further, it is clear from the above described experiments that the CO oxidation on Pt results from both H_2O and O_2 permeating from the cathode. These are discussed next.

CO oxidation mechanism and kinetics.—There is still considerable controversy concerning the CO oxidation mechanism in fuel cells. It is commonly accepted, however, that the electrochemical CO oxidation in acidic solutions involves a surface reaction between adsorbed CO molecules and an oxygen-containing species,[16] the exact nature of which is as yet unclear. Markovic *et al.*[17,18] and Gasteiger *et al.*,[9,10] based on their extensive work on CO electro-oxidation in liquid electrolytes in the absence of molecular oxygen, suggest that CO_{ad} oxidation on Pt follows the same mechanism both in the preignition region and ignition potential region in cyclic voltammetry, and involves reaction with OH_{ad},[17] *i.e.*

$$\text{Pt-OH} + \text{Pt-CO} \rightarrow 2\text{Pt} + CO_2 + H^+ + e^- \qquad [5]$$

Cyclic voltammetry and spectroscopic studies reveal that both the formation of oxygen-containing species and the CO oxidation reaction are potential dependent, and the reversible adsorption of OH_{ad} occurs in the potential range 0.7-0.8 V *vs.* reversible hydrogen electrode (RHE) in liquid sulfuric acid electrolyte.[17-19] In a Fourier transform infrared (FTIR) study by Iwasita *et al.*,[19] the lowest potential where the 3270 cm^{-1} peak appears, which is characteristic of OH_{ad}, is 0.7 V, although they proposed that the water dissociation to form OH_{ad} may begin at around 0.5 V. The cyclic voltammetry studies with PEM fuel cell at 80°C also indicate that the ignition potenial of the CO oxidation peak is in the range of 0.6–0.7 V,[20,21] believed to be due to the appreciable formation of surface OH_{ad} species. However, Markovic *et al.*[17] argue that OH_{ad} can also be formed at low overpotentials on the step/defect sites, such as those on Pt(100) surface. The nominal value of this defect concentration is on the order of 10^{12}-10^{13} per cm^2, which is less than 1% of the total number density of surface sites.[18] Thus, although the occurrence of OH_{ad} on the Pt surface at low overpotentials is also possible, it is apparent that appreciable surface coverage of OH_{ad} occurs only at higher overpotentials. So there is the possibility that in the low-potential region the oxygen-containing species may be other than OH_{ad}. A similar conclusion is reached by other researchers such as Ciureanu *et al.*[20] and Bush *et al.*[22] Despite this controversy, it is evident that there is a marginal CO electro-oxidation on the Pt surface even before the significant CO electro-oxidation occurs at higher overpotential.

Based on above discussions as well as the modeling work of Springer *et al.*[23,24] and Ticianelli *et al.*,[25] we adopt the following reduced mechanism solely for the purpose of writing kinetics of H_2 and CO electro-oxidation on Pt surface

$$\text{CO} + \text{Pt} \leftrightarrows \text{Pt-CO} \quad k_{ac},\ K_C \qquad [6]$$

$$H_2 + 2\text{Pt} \leftrightarrows 2\text{Pt-H} \quad k_{ah},\ K_H \qquad [7]$$

$$\text{Pt-H} \rightarrow \text{Pt} + H^+ + e^- \quad k_{oh} \qquad [8]$$

$$\text{Pt-CO} + H_2O \rightarrow \text{Pt} + CO_2 + 2H^+ + 2e^- \quad k_{oc} \qquad [9]$$

where k_{ac} and k_{ah} are the adsorption rate constants of CO and H_2, respectively, K_C and K_H are the corresponding equilibrium constants for desorption of CO and H_2 (the reciprocal of the adsorption equilibrium constant). Similarly, k_{oc} and k_{oh} are the rate constants of the electro-oxidation of CO and H_2, respectively. Reaction 9 is clearly not an elementary step, but is rather the overall reaction of CO electro-oxidation via water.

It is also evident from the experimental results of this study that oxygen diffusing from the cathode to the anode is partly responsible for the CO oxidation in the anode side. This is in agreement with literature results that bleeding a small amount of O_2 or air into the anode feed stream is effective in mitigating the CO poisoning of the PEM fuel cell anode.[3,14] One explanation for this is that CO is oxidized by O_2 via a nonelectrochemical surface redox mechanism, for instance

$$O_2 + 2\text{Pt} \leftrightarrows 2\text{Pt-O} \qquad [10]$$

$$\text{Pt-O} + \text{Pt-CO} \rightarrow 2\text{Pt} + CO_2 \qquad [11]$$

which is similar, in principle, to the preferential oxidation (PrOx) process.[26] Another possibility is that adsorbed O reacts first with adsorbed H to form OH_{ad} that further reacts with surface CO electrochemically as per Reaction 5

$$\text{Pt-O} + \text{Pt-H} \leftrightarrows \text{Pt-OH} \qquad [12]$$

In summary, the mechanism of CO oxidation by molecular O_2 on Pt/C anode catalyst at temperatures below 100°C is also not clear.[27,28]

Of course, there is little doubt that the adsorbed oxygen reacts with adsorbed hydrogen to form water as well. Therefore, only part of the oxygen diffusing across the membrane to the anode would participate in CO oxidation. This is accounted for simply by β, the selectivity parameter for CO oxidation in our model.

The model provided by Springer *et al.*[24] is adopted here for the anode kinetics which is based on the mechanism described by Eq. 6 to 9. The rate expression for H_2 oxidation, which is also the overall fuel cell current density, is obtained from Eq. 8 and assumed to obey the Butler-Volmer equation

$$i = 2k_{oh}\theta_H \sinh\left(\frac{\alpha_H F \eta_A}{RT}\right) \qquad [13]$$

while the CO electro-oxidation current based on Eq. 9 is expressed in a Tafel form[24]

$$i_{CO} = k_{oc}\theta_{CO} \exp\left(\frac{\alpha_{CO} F \eta_A}{RT}\right) \qquad [14]$$

In this expression, Springer *et al.*[24] assume the concentration of the oxidizing species to be constant and included in rate constant k_{oc}. Here α_{CO} is the effective transfer coefficient for CO electro-oxidation, and i_{CO} denotes the CO electro-oxidation current density. Both k_{oc} and α_{CO} are treated here as fitted parameters. Furthermore, Eq. 13 and 14 imply absence of mass-transfer limitations.

The hydrogen adsorption as per Eq. 7 is assumed to be second order in vacant sites coverage, $\theta_0 = 1 - \theta_{CO} - \theta_H$. Detailed dis-

Table I. Model parameters.

K_{CO}	2×10^{-6} atm	CO desorption equilibrium constant[a]
K_H	0.5 atm	H_2 desorption equilibrium constant[a]
α_H	1.0	Transfer coefficient for H_2[a]
α_{CO}	0.12	Transfer coefficient for CO[c]
k_{ah}	40.21 A cm^{-2} atm^{-1}	Adsorption rate constant of H_2[a]
k_{ac}	10 A cm^{-2} atm^{-1}	Adsorption rate constant of CO[a]
T	353 K	Fuel cell temperature
k_{oh}	4.0 A cm^{-2}	Electro-oxidation rate constant for H_2[a]
k_{oc}	7×10^{-6} A cm^{-2}	Electro-oxidation rate constant for CO[c]
A	5 cm^2	Electrode active area
P_{H_2}	2.53 atm	Hydrogen partial pressure
x_{CO}	108×10^{-6}	CO mole fraction in anode feed stream
D	8.7×10^{-6} cm^2 s^{-1}	O_2 diffusion coefficient in Nafion at 80°C[b]
K	8.86×10^{-7} mol cm^{-3} atm^{-1}	Henry's law constant for O_2 dissolution in Nafion at 80°C[b]
β	0.04	O_2 selectivity[c]
L	0.01 cm	Thickness of Nafion 115 membrane in MEA under fuel cell operating conditions

[a] From or calculated from Ref. 24.
[b] From or calculated from Ref. 29.
[c] Fitted parameters.

cussion of this can be found in Springer *et al.*'s work.[24] The surface coverages of CO and H_2 are determined by their adsorption, desorption, and electro-oxidation rates. Thus at steady state, the surface coverages of CO and H do not change with time, *i.e.*

$$\rho \frac{d\theta_{CO}}{dt} = k_{ac} p_{H_2} x_{CO}(1 - \theta_{CO} - \theta_H) - K_C k_{ac} \theta_{CO} - k_{oc} \theta_{CO} \exp\left(\frac{\alpha_{CO} F \eta_A}{RT}\right) = 0 \quad [15]$$

$$\rho \frac{d\theta_H}{dt} = k_{ah} p_{H_2}(1 - \theta_{CO} - \theta_H)^2 - K_H k_{ah} \theta_H{}^2 - 2k_{oh} \theta_H \sinh\left(\frac{\alpha_H F \eta_A}{RT}\right) = 0 \quad [16]$$

where ρ is a constant, which equals to the moles of Pt per cm^2 electrode times the Faraday constant. All the values of model parameters are adopted from Springer *et al.*'s work[24] except α_{CO} and k_{oc} are fitted (see Table I). For k_{ah} and K_C, their values corresponding to high CO surface coverage are used here.

Oxygen permeation.—It is assumed that the oxidation of CO by permeating O_2 from cathode is controlled by the rate of permeation of O_2 through the membrane, the oxidation kinetics themselves being rapid. Further, we use a parameter β, which accounts for the selectivity of the oxygen for the oxidation of CO, the balance fraction being utilized for oxidation of hydrogen. This parameter is comparable to the selectivity of O_2 in PrOx of CO in a hydrogen-rich gas.[26]

Oxygen permeation in proton-exchange membranes is relatively well studied.[29-32] Parthasarathy *et al.*[29] determined the permeability of O_2 in Nafion at 80°C to be 3.85×10^{-11} mol cm^{-1} s^{-1}. Gottesfeld *et al.*[30] reported an O_2 concentration (solubility) of 3.1×10^{-6} mol cm^{-3} and a diffusion coefficient of 4.0×10^{-6} cm^2 s^{-1} at 25°C. Ogumi *et al.*[31, 32] used a transient method to measure the O_2 permeation in different membranes. Their result shows that the O_2 solubility in Nafion at 50°C is 5.9×10^{-6} mol cm^{-3}, and the diffusion coefficient is 5.2×10^{-7} cm^2 s^{-1}.

At steady state, we assume that the partial pressure of oxygen approaches zero at the anode-membrane interface due to rapid kinetics and rate limitations by mass transfer through the proton-exchange membrane. Under steady-state diffusion conditions, the flux of O_2 can thus be expressed as

$$N_{O_2} = \frac{KDP_{O_2}}{L} \quad [17]$$

where D is the diffusion coefficient of O_2 in Nafion membrane, L is the thickness of the membrane under operation, K is the Henry's law constant for O_2 dissolution in Nafion membrane at 80°C, p_{O_2} is the partial pressure of O_2 at the proton-exchange membrane surface at the cathode side. For simplicity, it is further assumed here that this corresponds to cathode chamber partial pressure of O_2, any difference being accounted for by β.

CO inventory model.—Since CO is in trace amounts, it does not contribute materially to the flow rate at the anode inlet or outlet. At a constant current density, a definite amount of H_2 is consumed at the anode. The H_2 in excess of the stoichiometry flows out at the anode outlet. Since the CO electro-oxidation rate is inherently small compared to H_2 electro-oxidation, its contribution to the overall current density is negligible as well. Furthermore, the CO and H_2 diffusion limitations through the diffusion layer and catalyst layer are also assumed to be negligible, as discussed earlier. In other words, the CO and H_2 partial pressures at the Pt surface are the same as that in the anode chamber.

Equation 4 as applied to H_2 in the anode chamber at steady state provides

$$\frac{p_0 v_0}{RT_0} - \frac{p_0 v}{RT_0} = \frac{i}{2F} A \quad [18]$$

here F is the Faraday constant and i is given by Eq. 13. Note that the volumetric flow rates are measured at 1 atm and 298 K, so that p_0 is 1 atm and T_0 is 298 K, and not the fuel cell operating pressure or temperature.

Utilizing Eq. 4 for CO inventory in the anode

$$\frac{p_0 v_0}{RT_0} x^0{}_{CO} - \frac{p_0 v}{RT_0} x_{CO} = \left(\frac{i_{CO}}{2F} + 2\beta N_{O_2}\right) A \quad [19]$$

where $x^0{}_{CO}$ and x_{CO} are the CO mole fractions in the anode feed and the anode compartment outlet, respectively. β is assumed here to be

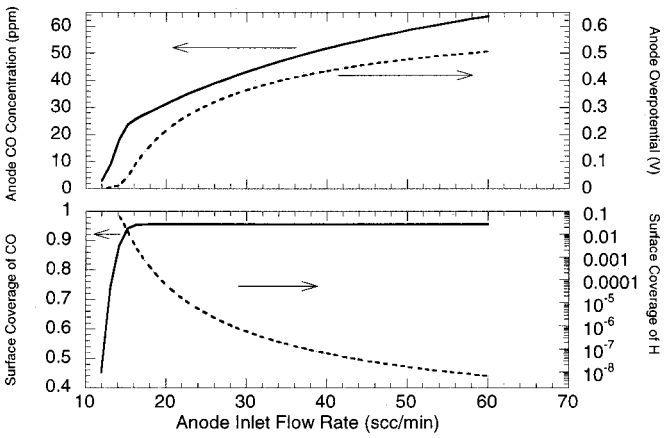

Figure 10. Model prediction of the steady-state CO and H surface coverage, CO content in anode chamber and the anode overpotential as a function of anode inlet flow rate at 80°C and 200 mA/cm^2; model parameters have values given in Table I.

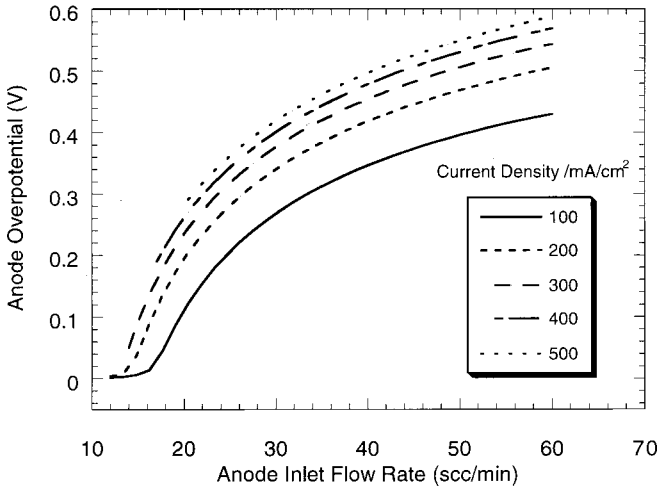

Figure 11. Model calculations of the steady-state anode overpotential as a function of anode inlet flow rate at 80°C and different current densities. Model parameters values are given in Table I.

a fitted constant. The right side of Eq. 19 accounts for the CO oxidized both electrochemically via water (Eq. 9) and nonelectrochemically via permeating O_2 (Eq. 11).

The input parameters for the model are the given anode inlet flow rate v_0 and the constant current density i. The corresponding value of θ_{CO}, θ_{H_2}, x_{CO}, η_A are then solved from the set of nonlinear Eq. 13-19 using Berkley-Madonna software, and plotted as a function of the anode inlet flow rate v_0.

Modeling results and discussion.—Figure 10 shows modeling results of the surface coverage of H and CO, θ_H and θ_{CO}, anode overpotential, η_A, and anode CO content, x_{CO} as a function of the anode inlet flow rate v_0 at $i = 200$ mA/cm^2 and 80°C. It is seen from these results that for the set of assumed parameters (Table I), the surface coverage of CO increases rapidly to an equilibrium value and does not change appreciably with a further increase of the anode flow rate and the corresponding increase in x_{CO}. As expected, the surface is largely covered by CO, being nearly a monolayer, which is consistent with the literature.[7] This feature is due to the large CO adsorption equilibrium constant on Pt. The hydrogen surface coverage decreases with the flow rate, while the anode overpotential increases as indicated in the figure, so the current density i can remain constant at the desired value (Eq. 13). It is also seen that the hydrogen surface coverage can be several orders of magnitude lower than the CO coverage. However, even this exceedingly small surface coverage can sustain a large current density due to the very large H electro-oxidation rate constant. The increase in anode overpotential η_A with the anode flow rate is qualitatively similar to the experimental results. The simulation also shows that the CO content x_{CO} in the anode chamber increases with the inlet flow rate as expected, and is the key reason for increased poisoning at higher flow rates. This simple inventory model here thus reproduces the essential features of the experimental observations. The simulation confirms the observed form of dependency of anode overpotential on the flow rate.

Figure 11 shows the simulation results for the anode overpotential change as a result of the change of anode inlet flow rate at different current densities. At larger current densities, the overpotential is higher. The maximum overpotential change from about 0.4 V at 100 mA/cm^2 to 0.60 V at 500 mA/cm^2 is similar to the experimental results (see Fig. 5). Further, the modeling results qualitatively reproduce the S-shaped curve at smaller current densities, *e.g.*, at 200 mA/cm^2.

The simulation results for different cathode oxygen pressures are shown in Fig. 12, which demonstrates that the anode overpotential increases with the decrease of the cathode oxygen pressure at a certain anode flow rate. The predicted trend of the polarization curve is in good quantitative agreement with the experimental results for different cathode O_2 pressures (Fig. 7). The value of the selectivity β used in this simulation is 0.04, which is in the range indicated in the literature. Gottesfeld *et al.*[3] found that by injecting 2-5% O_2 into the anode stream, a complete performance recovery could be achieved for an anode feed with H_2 containing 100-500 ppm CO. This indicates a selectivity on the order of 0.01.

The given CO inventory model, thus, adequately justifies the observed experimental phenomena of the effects of flow rate and oxygen permeation even though there is not an exact correspondence between theory and experiments. At small anode flow rates, the CO content in the anode compartment is low as it is consumed by electro-oxidaton and nonelectro-oxidaton. The slow increase of anode overpotential is due to the fact that the marginal oxidation or electro-oxidation of CO at low flow rates creates adequate bare Pt sites to sustain the desired current. As the inlet flow rate further increases, the anode chamber CO content becomes higher and the surface coverage of CO tends to increase as kinetics are unable to oxidize all CO coming in, unless the anode overpotential is in-

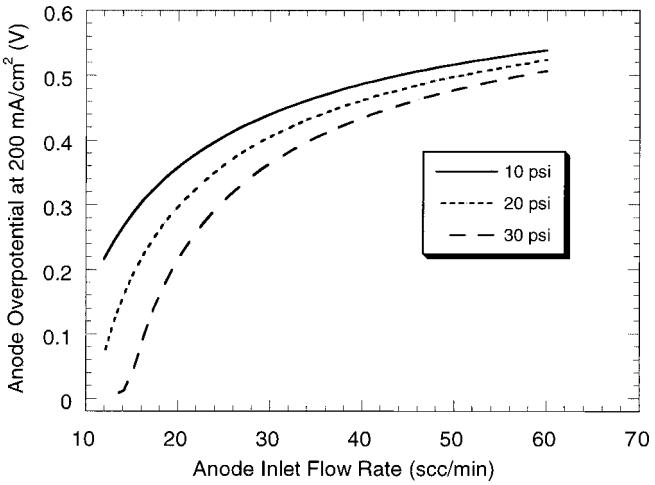

Figure 12. Model calculations of the steady-state anode overpotential as a function of anode inlet flow rate for different cathode O_2 pressures at 80°C and 200 mA/cm^2. Model parameter values are given in Table I.

creased correspondingly to accelerate the CO electro-oxidation rate and sustain the current density. When the overpotential is high enough, the CO electro-oxidation rate is fairly large compared to the inlet flow rate of CO, so that a plateau is reached and further increase of the anode overpotential is not necessary.

Even though the simple model described here is able to qualitatively explain the experimental observations, further work is needed to confirm the kinetics and the parameter values so as to obtain quantitative agreement with experiments.

Conclusions

The anode flow rate and cathode oxygen partial pressure are important operational parameters that strongly influence the performance of a PEM fuel cell involving a Pt anode when operating with H_2/CO feed. Cell voltage decreases dramatically with increasing anode flow rate at a constant current density due to increasing CO content in the anode chamber, requiring a higher anode overpotential to oxidize the adsorbed CO so as to sustain the desired current density. The influence of flow rate was found to be rapid and reversible. Oxygen diffusing through the membrane is partly responsible for the removal of CO on the anode catalyst surface. A CO inventory model is proposed which provides an adequate explanation of the observed effects of anode flow rate and cathode oxygen pressure. The CO oxidation hence needs to be included in the modeling of the overall fuel cell performance when reformate is used as the anode feed. A more detailed study of the mechanism and kinetics at the PEM fuel cell operating conditions for H_2/CO is necessary to obtain better quantitative agreement between theory and experiments.

Acknowledgments

We are grateful to Dr. Tom Springer of the Los Alamos National Laboratory for an insightful discussion on the effect of cathode oxygen permeation on anode polarization in the presence of CO. This work was partially supported by H Power Corporation under Naval Surface Warfare Center (NSWC) contract no. N00167-99-C-0002.

Worcester Polytechnic Institute assisted in meeting the publication costs of this article.

References

1. T. R. Ralph, *Platinum Met. Rev.*, **41**, 102 (1997).
2. T. R. Ralph, G. A. Hards, J. E. Keating, S. A. Campell, D. P. Wilkinson, M. Davis, J. St-Pierre, and M. C. Johnson, *J. Electrochem. Soc.*, **144**, 3845 (1997).
3. S. Gottesfeld and J. Pafford, *J. Electrochem. Soc.*, **135**, 2651 (1988).
4. H.-F. Oetjen, V. M. Schmidt, U. Stimming, and F. Trila, *J. Electrochem. Soc.*, **143**, 3838 (1996).
5. S. J. Lee, S. Mukerjee, E. A. Ticianelli, and J. McBreen, *Electrochim. Acta*, **44**, 3283 (1999).
6. G. K. Acres, J. C. Frost, G. A. Hards, R. J. Potter, T. R. Rulph, D. Thompsett, G. T. Burstein, and G. J. Hutchings, *Catal. Today*, **38**, 393 (1997).
7. R. J. Bellows, E. P. Marucchi-Soos, and D. T. Buckley, *Ind. Eng. Chem. Res.*, **35**, 1235 (1996).
8. R. J. Bellows and E. Marucchi-soos, in *Proton Conducting Membrane Fuel Cells II*, S. Gottesfeld and T. F. Fuller, Editors, PV 98-27, p. 218, The Electrochemical Society Proceedings Series, Pennington, NJ (1997).
9. H. A. Gasteiger, N. M. Markovic, and P. N. Ross, *J. Phys. Chem.*, **99**, 8290 (1995).
10. H. A. Gasteiger, N. M. Markovic, and P. N. Ross, *J. Phys. Chem.*, **99**, 16757 (1995).
11. H. P. Dhar, L. G. Christner, and A. K. Kush, *J. Electrochem. Soc.*, **134**, 3021 (1987).
12. H. P. Dhar, L. G. Christner, A. K. Kush, and H. C. Maru, *J. Electrochem. Soc.*, **133**, 1574 (1986).
13. J. K. Hong, L. A. Zook, M. Inbody, J. Tafoya, and N. E. Vanderborgh, Abstract 570, The Electrochemical Society Meeting Abstracts, Vol. 99-I, Seattle, WA, May 2-6, 1999.
14. J. W. Bauman, T. A. Zawodzinski, Jr., and S. Gottesfeld, in *Proton Conducting Membrane Fuel Cells II*, S. Gottesfeld and T. F. Fuller, Editors, PV 98-27, p. 136, The Electrochemical Society Proceedings Series, Pennington, NJ (1997).
15. T. Thampan, S. Malhotra, J. Zhang, and R. Datta, *Catal. Today*, **67**, 15 (2001).
16. S. Gilman, *J. Phys. Chem.*, **68**, 70 (1964).
17. N. M. Markovic, C. A. Lucas, B. N. Grgur, and P. N. Ross, *J. Phys. Chem.*, **103**, 9616 (1999).
18. N. M. Markovic, T. J. Schmidt, B. N. Grgur, H. A. Gasteiger, R. J. Belm, and P. N. Ross, *J. Phys. Chem. B*, **103**, 8568 (1999).
19. T. Iwasita and X. Xia, *J. Electroanal. Chem.*, **411**, 95 (1996).
20. M. Ciureanu and H. Wang, *J. Electrochem. Soc.*, **146**, 4031 (1999).
21. T. Zawodzinski, C. Karuppaiah, Y. Wu, S. Savett, F. Uribe, and S. Gottesfeld, Abstract 1098, The Electrochemical Society Meeting Abstract, Vol. 98-2, Boston, MA, Nov 1-6, 1998.
22. B. M. Bush, J. A. Reimer, and E. J. Cairns, *J. Electrochem. Soc.*, **148**, A137 (2001).
23. T. Springer, T. Zawodzinski, and S. Gottesfeld, in *Electrode Materials and Processes for Energy Conversion and Storage IV*, J. McBreen, S. Mukerjee, and S. Srinivasan, Editors, PV 97-13, p. 139, The Electrochemical Society Proceedings Series, Pennington, NJ (1997).
24. T. E. Springer, T. Rockward, T. A. Zawodzinski, and S. Gottesfeld, *J. Electrochem. Soc.*, **148**, A11 (2001).
25. E. A. Ticianelli, S. Mukerjee, S. J. Lee, and J. McBreen, in *Proton Conducting Membrane Fuel Cells II*, S. Gottesfeld and T. F. Fuller, Editors, PV 98-27, p. 162, The Electrochemical Society Proceedings Series, Pennington, NJ (1997).
26. M. J. Kahlich, H. A. Gasteiger, and R. J. Behm, *J. Catal.*, **171**, 93 (1997).
27. R. J. Bellows, E. Marucchi-Soos, and R. P. Reynolds, *Electrochem. Solid-State Lett.*, **1**, 69 (1998).
28. V. M. Schmidt, J. L. Rodriguez, and E. Pastor, *J. Electrochem. Soc.*, **148**, A293 (2001).
29. A. Parthasarathy, S. Srinivasan, and A. J. Appleby, *J. Electrochem. Soc.*, **139**, 2530 (1992).
30. S. Gottesfeld, I. D. Raistrick, and S. Srinivasan, *J. Electrochem. Soc.*, **134**, 1455 (1987).
31. Z. Ogumi, Z. Takehara, and S. Yoshizawa, *J. Electrochem. Soc.*, **131**, 769 (1984).
32. Z. Ogumi, T. Kuroe, and Z. Takehara, *J. Electrochem. Soc.*, **132**, 2601 (1985).